

On the role of mechanical feedback in synchronous to asynchronous transition during embryogenesis

Abdul N. Malmi-Kakkada^{*,1, a)} Sumit Sinha^{*,#, 2, b)} and D. Thirumalai^{2,3, c)}

¹⁾*Department of Physics and Biophysics, Augusta University, Augusta, GA 30912, USA*

²⁾*Department of Physics, University of Texas, Austin, TX 78712, USA*

³⁾*Department of Chemistry, University of Texas, Austin, TX 78712, USA*

(Dated: 1 December 2023)

Experiments have shown that during the initial stage of Zebrafish morphogenesis a synchronous to asynchronous transition (SAT) occurs, as the cells divide extremely rapidly. In the synchronous phase, the cells divide in unison unlike in the asynchronous phase. Despite the wide spread observation of SAT in experiments, a theory to calculate the critical number of cell cycles, n^* , at which asynchronous growth emerges does not exist. Here, using a model for the cell cycle, with the assumption that cell division times are Gaussian distributed with broadening, we predict n^* and the time at which the SAT occurs. The theoretical results are in excellent agreement with experiments. The theory, supplemented by agent based simulations, establish that the SAT emerges as a consequence of biomechanical feedback on cell division. The emergence of asynchronous phase is due to linearly increasing fluctuations in the cell cycle times with each round of cell division. We also make several testable predictions, which would further shed light on the role of biomechanical feedback on the growth of multicellular systems.

*Equal Contribution

#Present Address: Applied Mathematics (SEAS, Harvard University) & Data Science (Dana Farber Cancer Institute)

^{a)}Electronic mail: amalmikakkada@augusta.edu

^{b)}Electronic mail: ssinha@g.harvard.edu

^{c)}Electronic mail: dave.thirumalai@gmail.com

Time dependent synchronous behavior is pervasive across biological systems. Numerous examples of synchronous behaviors exist, from networks of neurons in the circadian pacemaker^{1,2}, and insulin-secreting pancreatic cells³ at the cellular scale, to the chirping of crickets⁴, and synchronous flashing of a colony of fireflies^{5,6}. A particularly fascinating example of tissue scale synchronous behavior occurs during the development of multicellular organisms, which proceeds through rapid and synchronous cleavage divisions that subdivide the fertilized egg into a large population of nucleated cells^{7,8}. For instance, a frog egg, divides into 37,000 cells in ~ 43 hours, while the *Drosophila* embryo proliferates to 50,000 cells in about 12 hours⁸. The early development of many animals is characterized by fast, synchronized divisions that occur are almost independent on inter cell interactions. This is followed by the midblastula transition accompanied by the loss of synchrony in cell division and a lengthening of the cell cycle^{7,9}.

The observation of spontaneous synchronization dates back to the 17th century when Christiaan Hyugens reported the synchronization of pendulums, due to transfer of energy from one to another. However, the reverse process of how asynchronous behavior emerges in a synchronous system is a fascinating question, with relevance to understanding morphogenesis in living systems. Given that cell collectives generate geometric order, driven predominantly by cell divisions and traction forces¹⁰, a better understanding the transition between synchronous to asynchronous cell division during early development of many animals could provide important insights into this process. Based on the analysis of the experimental data, coupled with theory and simulations, we show that the synchronous to asynchronous transition (SAT), during zebrafish morphogenesis, provides vital clues about how cells integrate biochemical and mechanical signals in regulating cell division.

Regulation of cell division is necessary for robust tissue growth and morphogenesis, with rapid cell proliferation being an integral phenotype characterizing early development^{11,12}. In cells that undergo cleavage divisions, maturation promoting factor (MPF) undergoes cyclical changes that drive mitosis^{8,13}. Biochemically, the cyclical activity of MPF is driven by the protein kinase, cyclin B, that accumulates during the DNA synthesis phase of the cell cycle, which is degraded once the cells reach the mitotic phase^{8,14,15}. In combination with the biochemical factors that regulate the cell behavior, changes in the embryonic physical properties can feed back onto biochemical dynamics¹⁶⁻¹⁸. In particular, mechanical pressure, built up due to rapid cell divisions may function as a feedback signal regulating cell division¹⁹.

Here, we discover that the SAT transition commonly observed during embryo development serves as a powerful example in dissecting the contribution of mechanical forces in controlling cell division. By analyzing experimental data, and developing theory and simulations of 3D multicellular collectives, we show that pressure experienced by cells due to mechanical interaction with their neighbors *quantitatively* explains the onset of the SAT. Furthermore, we predict that the lengthening of the cell cycle is a consequence of mechanical feedback on cell division.

Experimental Motivation: Our study is motivated by experimental data on time-dependent pattern of cell division during the early stages of Zebrafish morphogenesis. We start with a brief description of the experiment²⁰, which tracks the number of cell nuclei (a proxy for the number of cells), $N(t)$, as a function of time (t) using high-speed laser light-sheet fluorescence microscopy. Fig. 1a shows a plot of $N(t)$ as a function of t observed in the experiments. The cell divisions occur on the animal pole of the Zebrafish embryo (see inset showing three distinct division cycles), roughly every ~ 20 mins^{7,20}.

We focus on two distinctive features of the data. First, in the initial regime ($100 \text{ min} \leq t \leq 185 \text{ min}$), $N(t)$ exhibits a clear step-like pattern (see arrows in Fig 1a). Time intervals, with constant N , are interspersed with time regimes where the cell number increases (see the shaded regions). The step like pattern is a consequence of synchronous cell division, which is punctuated by finite time regimes where there are no cell division events. Second, at later times ($t \geq 185 \text{ min}$), the staircase pattern in $N(t)$ disappears, signaling the onset of the synchronous to asynchronous transition (SAT), which occurs at $n_E^* \sim 5$ rounds of cell division. Here, the subscript “E” denotes experiments. These interesting features of cell division raise the following questions: what sets the time scale at which the SAT transition occurs? and what, if any role, does biomechanical feedback plays on cell division in the SAT transition? These questions motivated us to first develop the theoretical framework.

Increasing fluctuations in cell division times drive the SAT: The experimental data²⁰ in Fig. 1a makes clear that the SAT occurs after $n_E^* \sim 5$ (the subscript E denotes experiments) rounds of cell division. Our objective is to provide a theory for predict the number of rounds, n_T^* (T stands for theory), it takes for the Zebrafish to exhibit SAT.

Let the n^{th} round of division for an individual cell occur at time, t_n . Assuming that t_n is

a random variable, we write it as,

$$t_n = \sum_{i=1}^n \tau_i, \quad (1)$$

where τ_i is the cell cycle time for the i^{th} round of cell division (see Fig. 2 in the SI). We assume that all the τ_i 's are independent and identically distributed random numbers with the statistics of τ_i 's being given by $\tilde{\mathcal{P}}(\tau)$ as derived in section I in the SI. From Eqn.(1), we can readily obtain the statistics of t_n . We will focus on the mean (μ_{t_n}) and the variance ($\sigma_{t_n}^2$) because they can be compared to the experimental data^{20,21}. The mean, μ_{t_n} , is given by

$$\mu_{t_n} = \sum_{i=1}^n \mu_{\tau,i} = n\mu_{\tau}, \quad (2)$$

and the variance, $\sigma_{t_n}^2$, is given by

$$\sigma_{t_n}^2 = \sum_{i=1}^n \sigma_{\tau,i}^2 = n\sigma_{\tau}^2. \quad (3)$$

Here, μ_{τ} and σ_{τ} are the mean and standard deviation of a single cell cycle round (see SI section I for details). As can be seen from Eqs. (2) and (3), both the mean and the fluctuations (variance) increase linearly with the number of cell cycle rounds, n . Also, we predict that the probability distribution for t_n , $\mathcal{F}(t_n)$ given by

$$\mathcal{F}(t_n) = \mathcal{N}(t_n; n\mu_{\tau}, \sqrt{n}\sigma_{\tau}), \quad (4)$$

where \mathcal{N} is a normal distribution with mean $n\mu_{\tau}$, and standard deviation $\sqrt{n}\sigma_{\tau}$.

To test the theoretical predictions, we quantified the statistics of cell cycle times from the experimental data. If our model is correct, we expect that the fluctuations in cell division times should increase at later cell division cycles. Remarkably, as predicted by theory (see Fig. 1) the variance increases as n increases. In Fig. 1b, we plot $\frac{dN}{dt}$ versus t , which allows us to extract the spread in cell division times for different n from the full width at half maximum (FWHM) of each peak (see Fig. 1b and inset). The spread in cell division times scales as $\sigma_{t_p} \propto n^{\frac{1}{1.6}}$, which is close to the theoretical prediction ($\sigma_{t_p} \propto n^{\frac{1}{2}}$). The modest deviation from theory might be due to poor statistics, suggesting that robust experiments should be performed to test the functional dependence of fluctuations with time. We note that Eq. (4) can be interpreted as a particle undergoing Brownian motion advected by a constant ‘‘velocity’’ μ_{τ} . Variability in cell cycle duration has been observed long ago, but

its origin is unclear^{22,23}. Our theory suggests that it is driven by fluctuations in cell division times.

With the ansatz for $\mathcal{F}(t_n)$, we can estimate n^* where SAT occurs. The onset of synchronous to asynchronous transition (SAT) corresponds to the absence of a plateau in the N as a function of t curves between successive cell division epochs. This is realized when the fluctuations in t_{n^*} are so large that the cell division time probabilities at two consecutive cell cycles - $\mathcal{F}(t_{n^*-1})$ and $\mathcal{F}(t_{n^*})$ - begin to overlap (see Figure 2a and 2b). Mathematically, this is equivalent to writing,

$$\mu_\tau \approx \lambda[\sigma_{t_{n^*-1}} + \sigma_{t_{n^*}}], \quad (5)$$

where λ controls the strength of the overlap between two successive distributions, \mathcal{F} 's. We assume that the two distributions start to overlap at three standard deviations from the mean, $\lambda = 3$ (see Fig. 2b). Note that λ can vary depending on the strength of the overlap between the cell division time probability distributions. Using $\lambda = 3$, we can calculate n^* , the cell cycle round when SAT occurs given by,

$$n^* = \left(\frac{\kappa^2 + 1}{2\kappa} \right)^2, \quad (6)$$

where $\kappa = \frac{\mu_\tau}{3\sigma_\tau}$. In the experiments, $\sigma_\tau = 1.6 \text{ min}$ and $\mu_\tau = 20 \text{ min}$. Therefore, $n^* = 4.85 \approx 5$ from Eqn. (6) (refer to Figure 3 in SI for dependence of n^* on λ), close to the experimental data in Figure 1a, where the transition occurs after five cell division rounds. The theory also predicts that at the transition, $\sigma_{t_{n^*}} = \sqrt{5}\sigma_{t_{n=1}} = 3.6 \text{ min}$, which is close to the experimentally observed value of 2.8 min . The choice of $\lambda = 3$ is justified *a posteriori*.

Step-like pattern in cell number growth is recapitulated in theory: The theory also captures the step-like pattern in the growth of $N(t)$ observed in experiments (see Figure 1a). We estimate that $N(n, t)$ which denotes the number of cells at time t after n rounds of cell division from the following relation,

$$N(n, t) = N(n-1, t)[1 + \xi(n, t)], \quad (7)$$

where $\xi(n, t)$ is the probability that a cell has undergone n rounds of cell division until time t . In particular, $\xi(n, t)$ is the cumulative distribution function (CDF) associated with $\mathcal{F}(t_n)$ is given by,

$$\xi(n, t) = \int_{-\infty}^t \mathcal{N}[s; \mu_{t_n}, \sigma_{t_n}] ds = \frac{1}{2} \left[1 + \text{erf} \left(\frac{t - \mu_{t_n}}{\sqrt{2}\sigma_{t_n}} \right) \right], \quad (8)$$

where erf is the error function. In the above equation, the lower integration limit is from $-\infty$ because the support of the normal distribution is from $[-\infty, \infty]$. However, since the standard deviation, σ_{t_n} , is small compared to μ_{t_n} , the majority of the contribution to integral in Eq. 8 arises from $[\mu_{t_n} - 3\sigma_{t_n}, \mu_{t_n} + 3\sigma_{t_n}]$. Substituting the expression for $\xi(n, t)$ into Eq. 7, we obtain the recursive relation,

$$N(n, t) = N(n - 1, t) + \frac{N(n - 1, t)}{2} \left[1 + erf\left(\frac{t - \mu_{t_n}}{\sqrt{2}\sigma_{t_n}}\right) \right]. \quad (9)$$

Since the initial condition, $N(n = 0, t = 0)$ is known, we can calculate $N(n, t)$ for any n and t . Remarkably, Figure 2c, which shows the plot for $N(n, t)$ as a function of t using Eqn. (9), reproduces the step-like pattern observed during Zebrafish morphogenesis (compare to Figure 1a and Figure 2c).

An essential question in cell biology is whether cell cycle control is deterministic or stochastic²⁴, and whether the observed variability in division times originate mainly from stochasticity, or from deterministic processes that appear to be random^{23,25}. Although the theory shows that synchronous cell division may be quantitatively described without considering interactions between cells, the onset of asynchronous cell division, with increasing cell numbers, points to the importance of the local physical forces experienced by cells upon division^{19,26,27}. Indeed, seminal studies have demonstrated that variations in cell density control cell proliferation rate through contact inhibition of proliferation²⁸. Contact inhibition is thought to restrict cell proliferation when space is limited with dense spatial arrangements of cells leading to strong suppression of cell division^{29,30}. To determine whether such mechanical effects influence SAT, we turn to a three-dimensional (3D) computational model for cell divisions.

Biomechanical feedback controls the SAT: Cells that are constantly in contact with their neighbors experience compressive forces that limit their ability to progress through the cell cycle. The cumulative effect of such compressive forces from the cell microenvironment can be characterized at the multicellular scale through pressure experienced by the cells. Such cell-cell contact-induced pressure is expected to decrease the rate of division^{19,21,27}. The possibility of mechanical feedback on cell division has significant implications, because cell cycle regulation is important in stem cell biology as pluripotent cells divide slowly over long periods but can initiate growth on demand. To capture these effects, we performed particle-based simulations^{27,31-36}, to investigate how cell cycle progression, controlled via feedback

based on local inter-cellular mechanical interactions, impacts the ability of cells to grow and divide. The cell cycle time during each round of cell division is μ_τ . Cells may divide only if pressure experienced by a cell is below a critical pressure ($p < p_c$). This implies that synchronous divisions occur during zebrafish morphogenesis before mechanical feedback is operative. The universality of SAT can be tested by conducting high temporal resolution cell cycle experiments on different cell types^{23,37}.

In our model, cells are either in the dormant (D) or in the growth (G) phase. Even though cells in the experiment do not grow, we consider physical cell growth as a proxy for cell cycle progression. We track the sum of the normal pressure, p_i that a particular cell i experiences due to contact with its neighbors, using

$$p_i = \sum_{j \in NN(i)} \frac{|\vec{F}_{ij} \cdot \vec{n}_{ij}|}{A_{ij}}, \quad (10)$$

where \vec{F}_{ij} is the force that i^{th} cell experiences from its nearest neighbors (NN) j , \vec{n}_{ij} is the unit vector that points from the center of cell j to the center of cell i , and the contact surface area between cells i and j is $A_{ij} = \pi h_{ij} R_i R_j / (R_i + R_j)$. The nearest neighbors of a cell is determined through positive overlap between cells through the h_{ij} , defined as $\max[0, R_i + R_j - |\vec{r}_i - \vec{r}_j|]$. Importantly, once the pressure exceeds the critical pressure p_c the cell stops growing and enters a dormant phase where cell division cannot occur. Lower p_c implies that cells enter the dormant phase with high probability while higher p_c values would make the cells less sensitive to feedback on division due to mechanical interactions with its neighbors. By varying p_c , we predict that higher sensitivity to mechanical feedback on cell growth leads to faster onset of asynchronous cell divisions. The growth rate of the cell collective closely recapitulate experimental data where clear peaks with bursts of cell division events followed by time regimes with absence of division events (see Figs. 3a-c). Notably, the synchronous division events are more persistent at higher p_c and are maintained for longer times as compared to lower p_c where the clear peaks in division rate are quickly washed out (compare Figs. 3a and c).

To quantify the synchronous nature of the cell division events, we evaluated the autocorrelation of the division rate to verify the presence of cycles and determine their duration. The autocorrelation function of a periodic signal has the same periodic characteristics, evaluated using,

$$C(t_\gamma) = \langle \Sigma_{\alpha,\beta} \frac{dN(t_\alpha)}{dt} \times \frac{dN(t_\beta)}{dt} \delta(t_\gamma - (t_\alpha - t_\beta)) \rangle, \quad (11)$$

where, t_γ is the lag time between time points t_α, t_β , and $\delta(z) = 1$ if $z = 0$ and 0 otherwise. The autocorrelation function is normalized to ensure that $C(t_\gamma = 0) = 1$. We focus on the first peak in the autocorrelation function in order to quantify the peak height and peak location as a function of p_c . The peak height measures the strength of the oscillatory division patterns. The peak height increases and saturates at high p_c , as shown in Fig. 3e, which is indicative of more persistent synchronous division patterns with weak mechanical feedback. (see Fig. 3f).

Mechanical feedback lengthens the cell cycle: So far we have focused on the collective effect of coordination of cell division events between different cells. We now delve into the single cell scale to verify our prediction that cell cycle lengthening is due to mechanical feedback. Many embryos exhibit a period of rapid cell division followed by a lengthening of cell division times during early development³⁸. The embryo developmental processes are crucially linked to the speed of cell division as well as the cell cytoskeleton during mitosis is engaged in building the mitotic spindle^{38,39}. As many of the morphogenetic events require cytoskeletal arrangements, they must wait for cell divisions to slow down³⁸. As such slowing of the cell division time, associated with the mid blastula transition, is an important and conserved feature of embryo development.

We anticipate that pressure-dependent feedback on cell division may lead to the lengthening of the cell cycle. Recently, we showed that pressure experienced by cells near the core of multicellular spheroids is elevated compared to those at the periphery, setting up emergent variations in the cell division rate between the core and periphery^{27,32,40}. Moreover, there is a the coupling between cell growth rate and pressure through intracellular molecular crowding was⁴¹. From the autocorrelation in cell growth rate (see Eq. 11), the lag time at which the peak is located is a measure of the time difference between two division events, which corresponds to the average cell cycle time. Our simulations show that the cell cycle time is inversely proportional to the value of the threshold pressure, p_c (see Fig 4a). Lower values of p_c correspond to higher sensitivity to cell division because mechanical forces exerted by cells on one another could easily reach a lower value of p_c (see Fig. 4b inset). Our quantification shows that higher sensitivity to mechanical feedback lead to a longer cell division time. We next turned to the experimental data to assess whether cell cycle lengthening is observed during Zebrafish development. Indeed, as shown in Fig. 4b, the cell cycle lengthens markedly as cells progress through repeated division cycles. Experimental data, therefore, shows that

SAT is followed by an increase in the mean cell cycle⁹ during Zebrafish morphogenesis. The data in this regime can be fit using $\mu_\tau(p, p_c) = \mu_\tau e^{\frac{p}{p_c}}$, where the exponential increase in cell cycle times is a consequence of mechanical feedback.

Conclusion The finding that synchronous cell division depends on the strength of mechanical feedback points to an interesting manifestation of the cross-talk between mechanical forces and cell cycle regulation during embryo development. Here, we showed that coordination between cells during cell cycle progression is regulated by whether cells experience strong or weak mechanical feedback. A direct implication of our study is that suppression of mechanical feedback, which may be realized by partial knockout of E-Cadherin, would prolong the synchronous phase. Given our prediction that asynchronized cell division emerge during the course of embryo development at the cusp of the mid-blastula transition, corresponding to the activation of transcription, SAT in cell division could be a signal for cells to trigger their own transcription programs as a function of increasing cell density. Cells that grow under strong mechanical feedback, transition rapidly into asynchronous cell division patterns even at very values of small pressure. In contrast, for cells growing under weak mechanical feedback, synchronous division patterns persist for a longer period of time.

We have shown that mechanical feedback drives the lengthening of the cell cycle time. Cells experiencing strong mechanical feedback elongate their cell cycle. On the other hand, cells under weak mechanical feedback progress through the cell cycle more rapidly and more uniformly. The proposed feedback mechanism on growth is therefore a ‘mechanical’ intercellular signal that enables cells to measure density and the timing of development.

The observation that embryos develop autonomously under a predetermined schedule is striking⁴²⁻⁴⁴. Studies based on molecular biology revealed that various genetic factors control the periodicity of the development of somites in which a network of genes whose expression oscillates synchronously and regulate the timing of development. As tissue mechanics was recently shown to be an important factor in the formation of body segments, formerly thought to be based on segmentation clock⁴⁵, we propose that mechanical feedback on cell growth serves as a clock (timing device) that mediates asynchronization of cell division, and therefore, the onset of the transcriptional machinery during the mid-blastula transition.

REFERENCES

- ¹Enright, J. T. Temporal precision in circadian systems: a reliable neuronal clock from unreliable components? *Science* **209**, 1542–1545 (1980).
- ²Mirollo, R. E. & Strogatz, S. H. Synchronization of pulse-coupled biological oscillators. *SIAM Journal on Applied Mathematics* **50**, 1645–1662 (1990).
- ³Sherman, A., Rinzel, J. & Keizer, J. Emergence of organized bursting in clusters of pancreatic beta-cells by channel sharing. *Biophysical journal* **54**, 411–425 (1988).
- ⁴Walker, T. J. Acoustic synchrony: two mechanisms in the snowy tree cricket. *Science* **166**, 891–894 (1969).
- ⁵Smith, H. M. Synchronous flashing of fireflies. *Science* **82**, 151–152 (1935).
- ⁶Sarfati, R., Hayes, J. C. & Peleg, O. Self-organization in natural swarms of photinus carolinus synchronous fireflies. *Science Advances* **7**, eabg9259 (2021).
- ⁷Kane, D. A. & Kimmel, C. B. The zebrafish midblastula transition. *Development* **119**, 447–456 (1993).
- ⁸Gilbert, S. F. An introduction to early developmental processes. In *Developmental Biology. 6th edition* (Sinauer Associates, 2000).
- ⁹Kimmel, C. B., Ballard, W. W., Kimmel, S. R., Ullmann, B. & Schilling, T. F. Stages of embryonic development of the zebrafish. *Developmental dynamics* **203**, 253–310 (1995).
- ¹⁰Gibson, M. C., Patel, A. B., Nagpal, R. & Perrimon, N. The emergence of geometric order in proliferating metazoan epithelia. *Nature* **442**, 1038 (2006).
- ¹¹Thompson, D. W. *et al.* On growth and form. *Cambridge Univ. Press* (1942).
- ¹²Shaw, T. J. & Martin, P. Wound repair at a glance. *Journal of cell science* **122**, 3209–3213 (2009).
- ¹³Gerhart, J., Wu, M. & Kirschner, M. Cell cycle dynamics of an m-phase-specific cytoplasmic factor in xenopus laevis oocytes and eggs. *The Journal of cell biology* **98**, 1247–1255 (1984).
- ¹⁴Evans, T., Rosenthal, E. T., Youngblom, J., Distel, D. & Hunt, T. Cyclin: a protein specified by maternal mrna in sea urchin eggs that is destroyed at each cleavage division. *Cell* **33**, 389–396 (1983).
- ¹⁵Swenson, K. I., Farrell, K. M. & Ruderman, J. V. The clam embryo protein cyclin a induces entry into m phase and the resumption of meiosis in xenopus oocytes. *Cell* **47**,

- 861–870 (1986).
- ¹⁶Samarage, C. R. *et al.* Cortical tension allocates the first inner cells of the mammalian embryo. *Developmental cell* **34**, 435–447 (2015).
- ¹⁷Maître, J.-L. *et al.* Asymmetric division of contractile domains couples cell positioning and fate specification. *Nature* **536**, 344–348 (2016).
- ¹⁸Gross, P., Kumar, K. V. & Grill, S. W. How active mechanics and regulatory biochemistry combine to form patterns in development. *Annu. Rev. Biophys* **46**, 337–356 (2017).
- ¹⁹Shraiman, B. I. Mechanical feedback as a possible regulator of tissue growth. *Proceedings of the National Academy of Sciences* **102**, 3318–3323 (2005).
- ²⁰Keller, P. J., Schmidt, A. D., Wittbrodt, J. & Stelzer, E. H. Reconstruction of zebrafish early embryonic development by scanned light sheet microscopy. *science* **322**, 1065–1069 (2008).
- ²¹Puliafito, A. *et al.* Collective and single cell behavior in epithelial contact inhibition. *Proceedings of the National Academy of Sciences* **109**, 739–744 (2012).
- ²²Smith, J. & Martin, L. Do cells cycle? *Proceedings of the National Academy of Sciences* **70**, 1263–1267 (1973).
- ²³Sandler, O. *et al.* Lineage correlations of single cell division time as a probe of cell-cycle dynamics. *Nature* **519**, 468–471 (2015).
- ²⁴Nurse, P. Cell cycle control—both deterministic and probabilistic? *Nature* **286**, 9–10 (1980).
- ²⁵Shields, R. Transition probability and the origin of variation in the cell cycle. *Nature* **267**, 704–707 (1977).
- ²⁶Irvine, K. D. & Shraiman, B. I. Mechanical control of growth: ideas, facts and challenges. *Development* **144**, 4238–4248 (2017).
- ²⁷Malmi-Kakkada, A. N., Sinha, S., Li, X. & Thirumalai, D. Adhesion strength between cells regulate nonmonotonic growth by a biomechanical feedback mechanism. *Biophysical Journal* **121**, 3719–3729 (2022).
- ²⁸Godard, B. G. & Heisenberg, C.-P. Cell division and tissue mechanics. *Current opinion in cell biology* **60**, 114–120 (2019).
- ²⁹Eagle, H. & Levine, E. M. Growth regulatory effects of cellular interaction. *Nature* **213**, 1102–1106 (1967).
- ³⁰Pavel, M. *et al.* Contact inhibition controls cell survival and proliferation via yap/taz-

- autophagy axis. *Nature communications* **9**, 2961 (2018).
- ³¹Malmi-Kakkada, A. N., Li, X., Samanta, H. S., Sinha, S. & Thirumalai, D. Cell growth rate dictates the onset of glass to fluidlike transition and long time superdiffusion in an evolving cell colony. *Physical Review X* **8**, 021025 (2018).
- ³²Sinha, S. & Thirumalai, D. Self-generated persistent random forces drive phase separation in growing tumors. *The Journal of Chemical Physics* **153**, 201101 (2020).
- ³³Sinha, S. & Malmi-Kakkada, A. N. Inter-particle adhesion regulates the surface roughness of growing dense three-dimensional active particle aggregates. *J. Phys. Chem. B* **125**, 10445–10451 (2021).
- ³⁴Sinha, S., Samanta, H. & Thirumalai, D. Observe without disturbing: tracer particles sense local stresses in cell collectives without affecting the cancer cell dynamics. *Soft Matter* **19**, 5385–5395 (2023).
- ³⁵Marchant, C. L., Malmi-Kakkada, A. N., Espina, J. A. & Barriga, E. H. Cell clusters softening triggers collective cell migration in vivo. *Nature Materials* **21**, 1314–1323 (2022).
- ³⁶Zills, G., Datta, T. & Malmi-Kakkada, A. N. Enhanced mechanical heterogeneity of cell collectives due to temporal fluctuations in cell elasticity. *Physical Review E* **107**, 014401 (2023).
- ³⁷Cermak, N. *et al.* High-throughput measurement of single-cell growth rates using serial microfluidic mass sensor arrays. *Nature biotechnology* **34**, 1052–1059 (2016).
- ³⁸Farrell, J. A. & O’Farrell, P. H. From egg to gastrula: how the cell cycle is remodeled during the drosophila mid-blastula transition. *Annual review of genetics* **48**, 269–294 (2014).
- ³⁹O Farrell, P. H. How metazoans reach their full size: the natural history of bigness. *Cold Spring Harbor Monograph Series* **42**, 1–22 (2004).
- ⁴⁰Sinha, S., Malmi-Kakkada, A. N., Li, X., Samanta, H. S. & Thirumalai, D. Spatially heterogeneous dynamics of cells in a growing tumor spheroid: Comparison between theory and experiments. *Soft Matter* **16**, 5294–5304 (2020).
- ⁴¹Alric, B., Formosa-Dague, C., Dague, E., Holt, L. J. & Delarue, M. Macromolecular crowding limits growth under pressure. *Nature Physics* **18**, 411–416 (2022).
- ⁴²Kageyama, R. 25 years of the segmentation clock gene (2022).
- ⁴³Perrimon, N., Pitsouli, C. & Shilo, B.-Z. Signaling mechanisms controlling cell fate and embryonic patterning. *Cold Spring Harbor perspectives in biology* **4**, a005975 (2012).

⁴⁴Artavanis-Tsakonas, S., Rand, M. D. & Lake, R. J. Notch signaling: cell fate control and signal integration in development. *Science* **284**, 770–776 (1999).

⁴⁵Naganathan, S. R., Popović, M. & Oates, A. C. Left–right symmetry of zebrafish embryos requires somite surface tension. *Nature* **605**, 516–521 (2022).

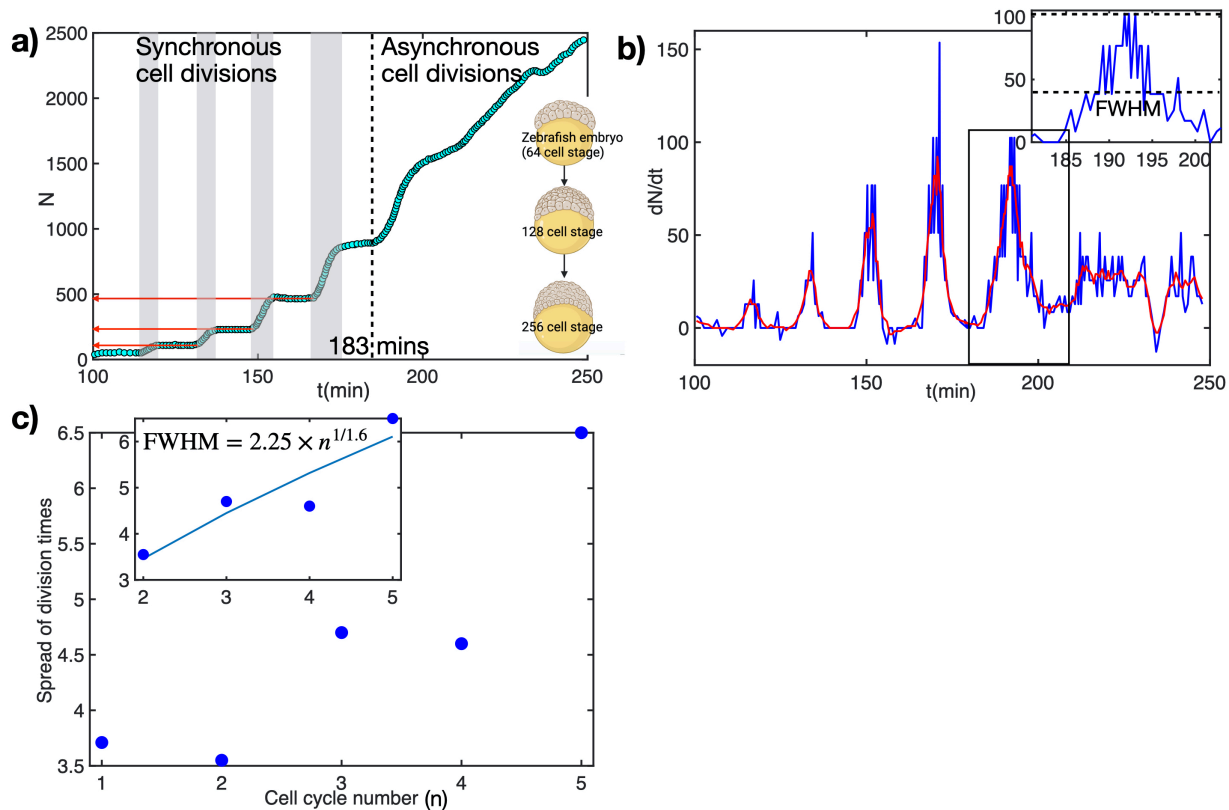


FIG. 1: Synchronous to asynchronous transition in cell division during embryo development

(a) Experimental data for the number of nuclei in the animal hemisphere of the Zebrafish embryo from the 64-cell stage to 2,000+ cells. Initially, cell divisions are highly synchronized (shaded portion) exhibiting staircase-like pattern in the time dependence of cell number growth. After roughly five cell division rounds, the asynchronous behavior sets in (at times past the dashed line), where the cell number increases essentially continuously, without the staircase pattern observed at early times. (b) The time derivative of $N(t)$ (growth rate) exhibits an oscillatory pattern where peaks indicate rapid cell division events and valleys represent time points where divisions do not occur. Peak widths, shown in the inset, is a measure of the heterogeneity in the cell cycle times. (c) Heterogeneity in the cell cycle time extracted from the full width at half maximum (FWHM) of the peaks associated with division events in (b). The FWHM increases as a function of the cell cycle number. The inset shows the fit to the data.

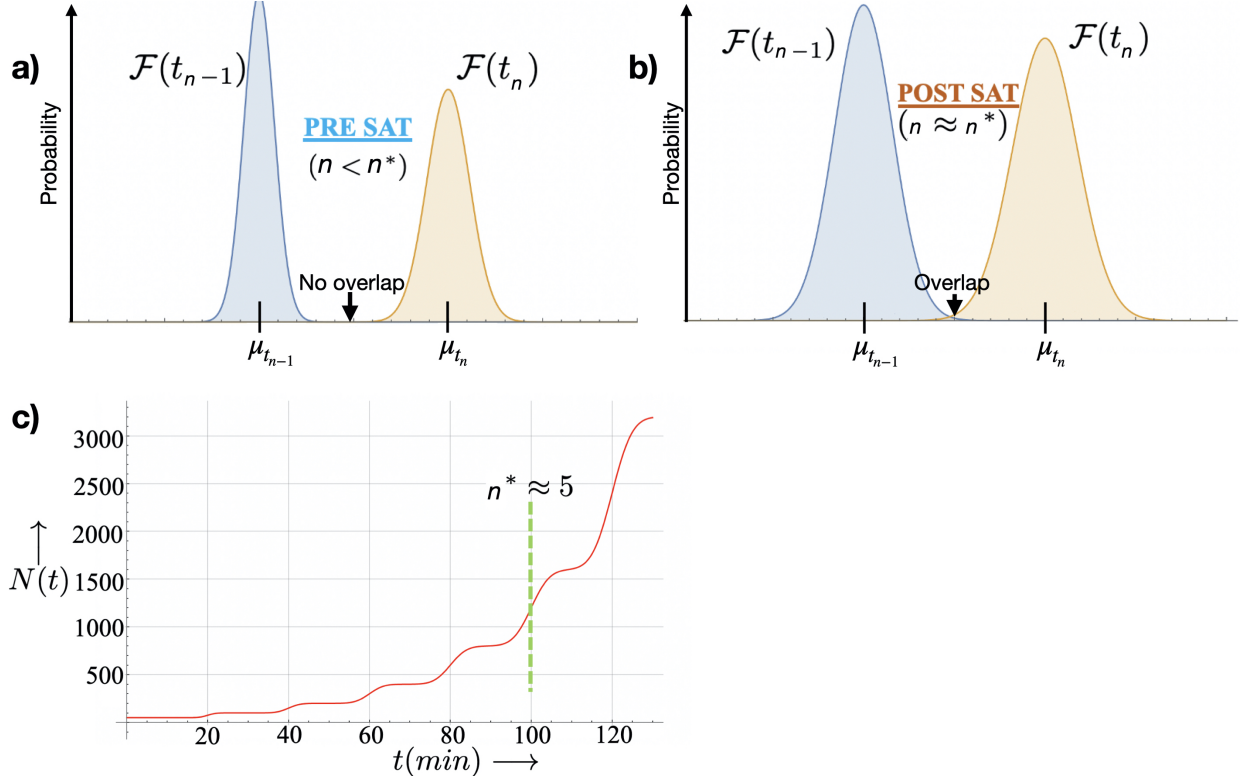


FIG. 2: **Variation in cell division times.** (a) Criteria used in the theory to predict the onset of the SAT in cell division. In the pre-SAT regime, the probability distributions, $\mathcal{F}(t_{n-1})$ and $\mathcal{F}(t_n)$ of the times at which cells divide, do not overlap, which implies that cells divide independently. (b) In the post-SAT regime, we propose that the distributions, $\mathcal{F}(t_{n-1})$ and $\mathcal{F}(t_n)$, begin to overlap, signaling the importance of cell-cell interactions. (c) Staircase-like pattern in N vs t curve calculated using theory. The plot shows the number of cells, $N(t)$, as a function of time (t) for multiple cell division rounds (n). The green dashed line demarcates the time at which SAT occurs resulting in $n^* \approx 5$. We reproduce the experimentally observed $N(t)$ vs t curves in Zebrafish Morphogenesis and the number of cell division cycles necessary for the onset of SAT⁹.

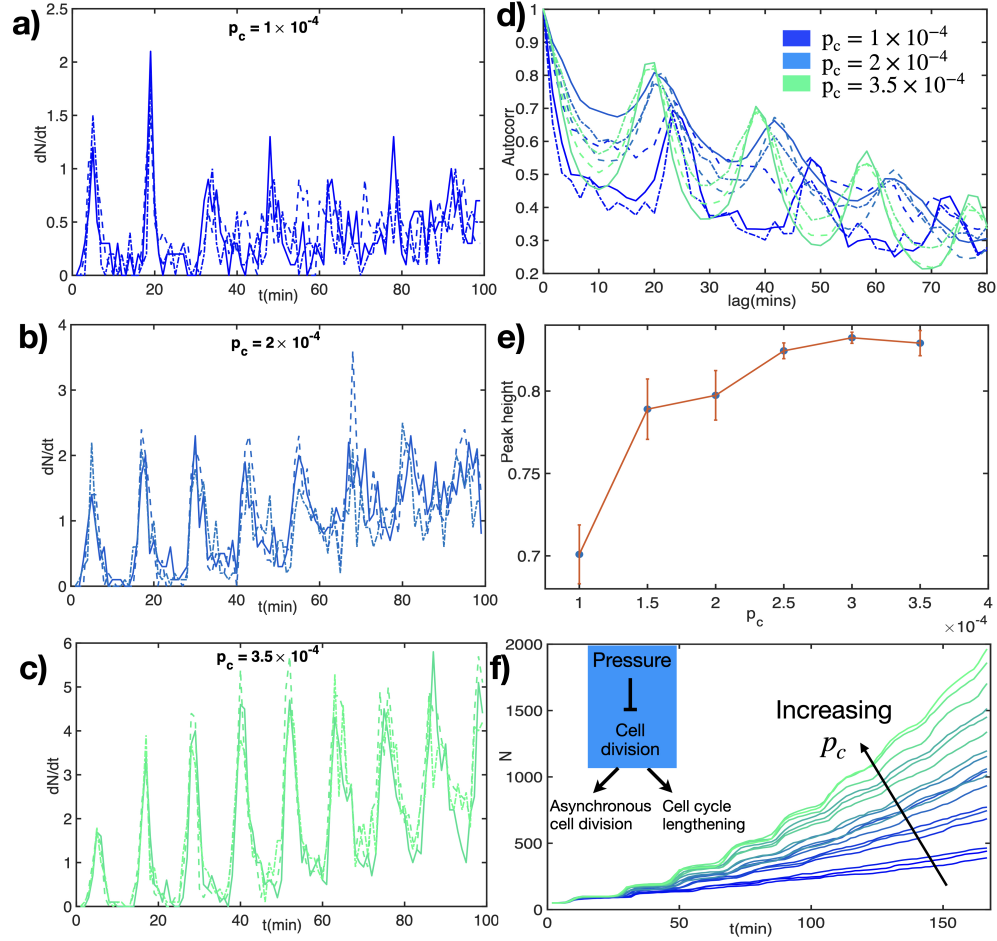


FIG. 3: Mechanical feedback determines synchronous cell division (a) Division rate as a function of time at low $p_c = 1 \times 10^{-4} MPa$. Low p_c value corresponds to heightened cell sensitivity to mechanical feedback on cell growth and division. (b-c) Division rate as a function of time at intermediate and high $p_c = 2.5 \times 10^{-4} MPa$ and $p_c = 3.5 \times 10^{-4} MPa$, respectively. Higher p_c value, corresponding to lesser cell sensitivity to mechanical feedback on cell growth and division, leads to highly synchronous cell division for a longer time range. (d) Autocorrelation of cell division rate at 3 p_c values. The height and time point of the first peak determine the strength of periodicity and the interval between repeated peaks in cell divisions. (e) Peak height of the autocorrelation function at varying sensitivity to mechanical feedback through pressure. Strength of periodic division rate increases with p_c and saturates at higher values. (f) Number of cells vs time as generated from simulations incorporating mechanical feedback on cell divisions. Inset: Schematic illustrating how increasing pressure limits cell divisions, leading to cell cycle lengthening and asynchronous cell divisions.

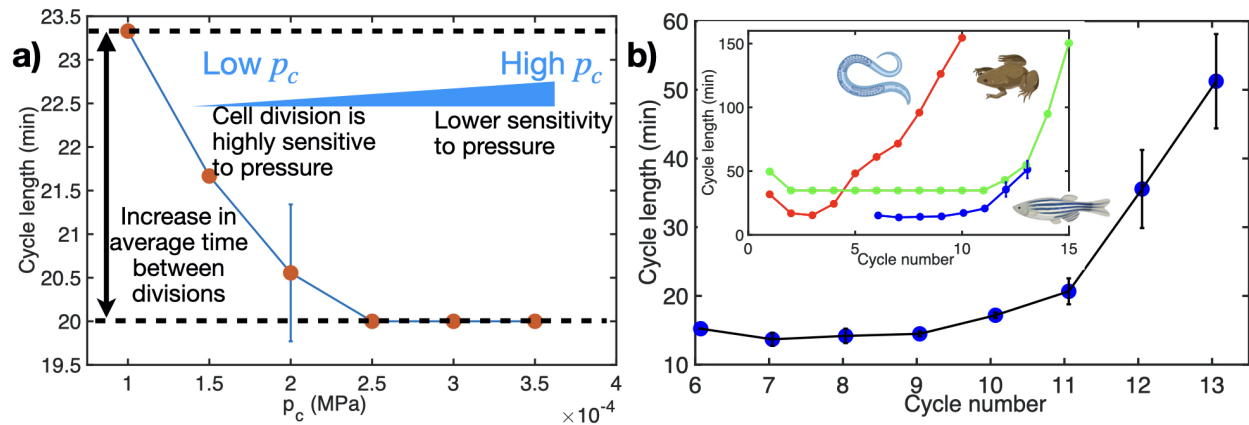


FIG. 4: **Mechanical feedback elongates cell cycle** (a) Average cell cycle length increases with stronger mechanical feedback. Cell cycle length is quantified from the time of the first peak in the growth rate autocorrelation function. (b) Experimental data extracted from Ref.⁷ for cell cycle length during cycle numbers 6-13 for Zebrafish development. Inset shows similar behavior that is conserved across multiple species - *C. elegans* (roundworm), *X. laevis* (frog) in addition to *D. rerio* (zebrafish).

Supplementary Information: On the role of mechanical feedback in synchronous to asynchronous transition during embryogenesis

Abdul N. Malmi-Kakkada,^{1, a)} Sumit Sinha,^{2, 3, 4, b)} and D. Thirumalai^{2, 5, c)}

¹⁾*Department of Physics and Biophysics, Augusta University, Augusta, GA 30192, USA*

²⁾*Department of Physics, University of Texas, Austin, TX 78712, USA*

³⁾*Applied Mathematics, School of Engineering and Applied Sciences, Harvard University, Cambridge, MA, USA*

⁴⁾*Department of Data Science, Dana-Farber Cancer Institute, Boston, MA, USA*

⁵⁾*Department of Chemistry, University of Texas, Austin, TX 78712, USA*

(Dated: 1 December 2023)

^{a)}Electronic mail: amalmikakkada@augusta.edu

^{b)}Electronic mail: ssinha@g.harvard.edu

^{c)}Electronic mail: dave.thirumalai@gmail.com

I. DISTRIBUTION FOR SINGLE CELL CYCLE DIVISION TIMES

The early embryonic cell cycles lack the layers of regulation that is present in more mature cells¹. To understand the role of mechanical feedback on cell cycle regulation, we introduce a minimal model. The multiple cell cycle stages, shown in Fig.S1a, are represented as discrete steps. Once a cell goes over all the stages, a cell undergoes division. Assuming that there are n stages, let us denote the i^{th} stage of a cell as G_i . We denote transition rate from $G_{n-1} \rightarrow G_n$ as k_n . We assume, for simplicity, that $k_1 = k_2 = \dots k_{n-1} = k$. The functional dependence of k on mechanical feedback (p) is given by,

$$k = \begin{cases} k & p \leq p_c \\ ke^{-\frac{p}{p_c}} & p > p_c \end{cases}, \quad (1)$$

where p is local mechanical stress on a cell, and p_c is the stress threshold value above which the cell is dormant, at least temporarily (see Fig. S1b). The functional form of k is inspired from experiments, where the cell division time increases as a function of tissue growth^{2,3}. For our model, the time (τ) it takes for a single cell to divide is given by,

$$\tau = \sum_{i=1}^{n-1} t_i, \quad (2)$$

where t_i is the transition time from G_{i-1} to G_i . Because the t_i 's are independent random variables, it follows that τ is a random variable as well. The assumption that $k_i = k$ for all i 's implies that the probability density of t_i 's, $\mathcal{P}(t_i)$, are identical, $\mathcal{P}(t_i) = \mathcal{P}(t)$. The probability density, $\mathcal{P}(t)$, is governed by the differential equation,

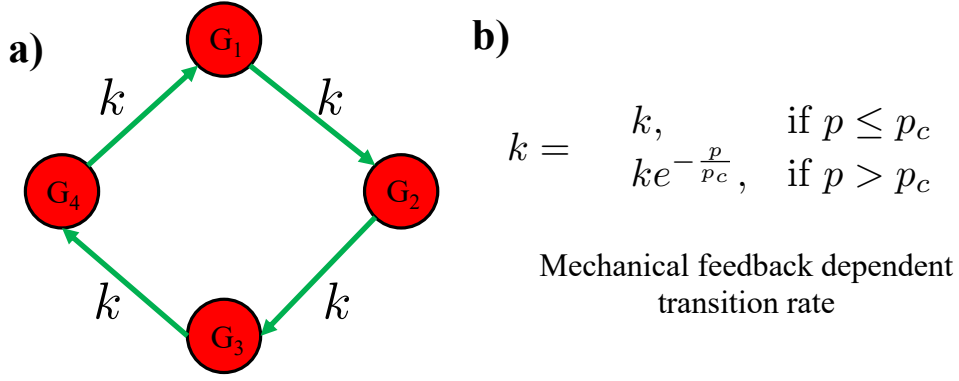
$$\frac{d\mathcal{P}(t)}{dt} = -k\mathcal{P}(t), \quad (3)$$

that is subject to the constraint $\int_0^\infty \mathcal{P}(t)dt = 1$. The solution to the above equation is,

$$\mathcal{P}(t) = ke^{-kt}. \quad (4)$$

By knowing the functional form of $\mathcal{P}(t)$, we can readily calculate all the moments of t . However, in this work, we focus on the mean and the variance as they are the relevant observables in the experiment⁴. The mean, $\mu_t = \langle t \rangle$, and the variance, $\sigma_t^2 = \langle t^2 \rangle - \langle t \rangle^2$, of $\mathcal{P}(t)$ are given as $\frac{1}{k}$ and $\frac{1}{k^2}$ respectively. Utilizing Eq. 2, we can calculate the mean (μ_τ) of the cell division time, τ , which is given by

$$\mu_\tau = \sum_{i=1}^n \mu_t = \frac{n}{k}, \quad (5)$$



Cell cycle

FIG. 1: **Schematic of stochastic model for cell division.** (a) Cartoon depicting a cell cycle for an individual cell. In the present picture, the cell cycle is assumed to be comprised of $n = 4$ stages (G_1, G_2, G_3, G_4). A single cell transitions from one stage to the other at the same rate, k . Once a cell has gone through all the stages, a cell is assumed to have undergone a single cell division. (b) The transition rate between the stages depends on mechanical feedback which is controlled by the local environment (see the expression for k given above).

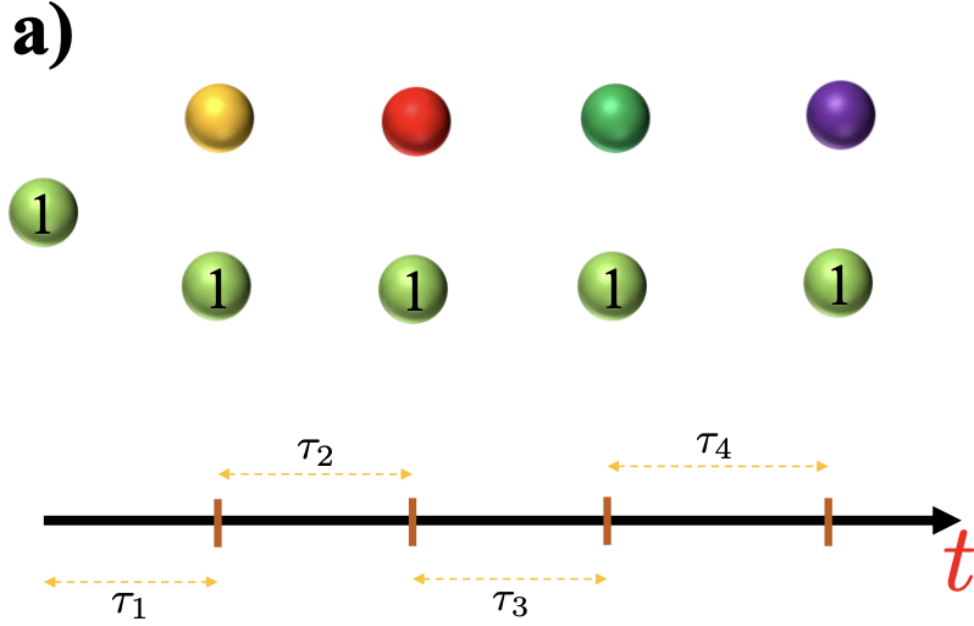
and the variance (σ_τ^2) of τ is

$$\sigma_\tau^2 = \sum_{i=1}^n \sigma_t^2 = \frac{n}{k^2}. \quad (6)$$

For zebrafish, $\mu_\tau \approx 20 \text{ min}$ and $\sigma_\tau \approx 1.6 \text{ min}^4$.

In order to analyze the experimental data, we fit the cell division times to a normal distribution (see Fig. 2a in the main text). Thus, for our analyses to be consistent with theory, we ought to recover the normal distribution from theory. This is possible in $n \rightarrow \infty$ limit, where we obtain $\tilde{\mathcal{P}}(\tau) = \mathcal{N}(\tau; \mu_\tau, \sigma_\tau)$ utilizing the well known central limit theorem. Here, $\tilde{\mathcal{P}}(\tau)$ denotes the probability distribution of cell division times τ , and $\mathcal{N}(\tau; \mu_\tau, \sigma_\tau)$ is the normal distribution with mean μ_τ and standard deviation σ_τ . Note that $\tilde{\mathcal{P}}(\tau)$ is the distribution of time, τ , for a cell to undergo a single cell division event.

Physiologically, $n \rightarrow \infty$ implies that for a cell to divide, numerous physio-chemical events have to be completed, which occurs with astonishing regularity in many organisms.



$$\begin{aligned}
 t_{p=1} &= \tau_1 \\
 t_{p=2} &= \tau_1 + \tau_2 \\
 t_{p=3} &= \tau_1 + \tau_2 + \tau_3 \\
 t_{p=4} &= \tau_1 + \tau_2 + \tau_3 + \tau_4
 \end{aligned}$$

FIG. 2: **Schematic of stochastic model for cell division.** The schematic for a cell (in green labelled as 1) undergoing subsequent cell divisions. The different colored cells at different time points are daughter cells. In the middle, a schematic for Eqn. 1 (main text) is shown. In the bottom, Eq. (1) (main text) is shown mathematically for different t_p , where p is the number of cell division rounds.

II. CHOICE OF λ

In Eq. 5 of the main text, we need the value of λ to predict the transition point. The parameter λ sets the degree of overlap between two cell division time probability distributions - $\mathcal{F}(t_{n^*-1})$ and $\mathcal{F}(t_{n^*})$. Figure 3 shows the plot of n^* as a function of λ . Approximately around $\lambda = 3$, we get the right fit between experiments and theory (see the main text).

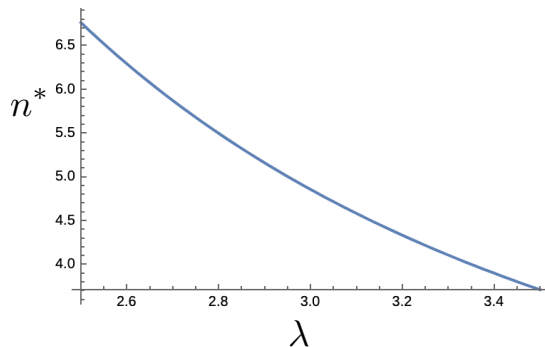


FIG. 3: Plot showing the dependence of n^* on λ .

III. SIMULATION DETAILS

Initial Conditions: At time, $t = 0$, we begin with 50 cells. The radii of the cells are sampled from a Gaussian distribution, $p(R_i) = \frac{1}{0.5\sqrt{2\pi}}e^{-(R_i-4.5)^2/2\times 0.5^2}$. Similarly, the elastic moduli, E_i and the Poisson ratio ν_i are obtained from a Gaussian distribution with standard deviation of 10^{-4} MPa and 0.02 respectively (the mean values are given in Table 1). The receptor and ligand concentration on the cell surface are Gaussian distributed ($p(c_i^{rec}/c_i^{lig}) = \frac{1}{0.02\sqrt{2\pi}}e^{-(c_i^{rec}/c_i^{lig}-0.9)^2/2\times 0.02^2}$), centered around the mean ($=0.9$) with a dispersion of 0.02. In subsequent cell division cycles, the daughter cell properties are sampled from the same distribution as described above. At each time step, the growth rate of the cell is also chosen from a Gaussian distribution.

Cell division: The volume of growing cells increases at a constant rate r_V . Cell radii are updated from a Gaussian distribution with the mean rate $\dot{R} = (4\pi R_m^2)^{-1}r_V$, and dispersion of 10^{-7} . Over the cell cycle time τ ,

$$r_V = \frac{2\pi(R_m)^3}{3\tau}, \quad (7)$$

where R_m is the mitotic radius. Table I lists the parameters used in the simulations.

TABLE I: Parameters used in the simulations.

Parameters	Values	References
Critical Radius for Division (R_m)	5 μm	5
Extracellular Matrix (ECM) Viscosity (η)	0.005 kg/($\mu\text{m s}$)	6
Benchmark Cell Cycle Time ($\tau_{min} = k_b^{-1}$)	900 s	7
Adhesive Strength (f^{ad})	$1 \times 10^{-4} \mu\text{N}/\mu\text{m}^2$	5, This paper
Mean Cell Elastic Modulus (E_i)	10^{-3}MPa	6
Mean Cell Poisson Ratio (ν_i)	0.5	5
Death Rate (k_a)	10^{-6}s^{-1}	This paper
Mean Receptor Concentration (c^{rec})	0.90 (Normalized)	5
Mean Ligand Concentration (c^{lig})	0.90 (Normalized)	5
Adhesive Friction γ^{max}	$10^{-4} \text{kg}/(\mu\text{m}^2 \text{s})$	This paper
Threshold Pressue (p_c)	$1.0 - 3.5 \times 10^{-4} \text{MPa}$	5,8

Cell-Cell Interactions: By building on our previous work⁹, we consider the cell-cell interactions to be driven by elastic (repulsive) and adhesive (attractive) forces. The total force on the i^{th} cell is, $\vec{F}_i = \sum_{j \in NN(i)} (F_{ij}^{el} - F_{ij}^{ad}) \vec{n}_{ij}$, where F_{ij}^{el} and F_{ij}^{ad} are cell-cell elastic and adhesive forces respectively, and \vec{n}_{ij} is the unit vector from the center of cell j to cell i . We used the Hertz contact mechanics^{5,10,11} to model the elastic forces between the spherical cells. R_i and R_j , are the cell radii and the parameters E_i and ν_i , respectively, are the elastic modulus and Poisson ratio of the i^{th} cell in the elastic force term: $F_{ij}^{el} = \frac{h_{ij}^{3/2}}{\frac{3}{4} \left(\frac{1-\nu_i^2}{E_i} + \frac{1-\nu_j^2}{E_j} \right) \sqrt{\frac{1}{R_i(t)} + \frac{1}{R_j(t)}}}$. The overlap between two cells, h_{ij} , is defined as $\max[0, R_i + R_j - |\vec{r}_i - \vec{r}_j|]$.

The inter-cell adhesive force, F_{ij}^{ad} , is given by,

$$F_{ij}^{ad} = A_{ij} f^{ad} \frac{1}{2} (c_i^{rec} c_j^{lig} + c_j^{rec} c_i^{lig}). \quad (8)$$

In the above equation, $A_{ij} = \pi h_{ij} R_i R_j / (R_i + R_j)$ is the cell-cell contact area, c_i^{rec} (c_i^{lig}) is the adhesion receptor (ligand) concentration (assumed to be normalized with respect to the maximum receptor or ligand concentration such that $0 \leq c_i^{rec}, c_i^{lig} \leq 1$)⁵. The dimensions of the adhesive strength, f^{ad} , in Eq. 8 is $\mu\text{N}/\mu\text{m}^2$.

Equations of Motion: If inertial effects are negligible⁹, the equation of motion of the

i^{th} cell is,

$$\dot{\vec{r}}_i = \frac{\vec{F}_i}{\gamma_i}, \quad (9)$$

where, $\gamma_i = \gamma_i^{\alpha'\beta',visc} + \gamma_i^{\alpha'\beta',ad}$ is the total friction coefficient. The cell-to-matrix friction is given by,

$$\gamma_i^{\alpha'\beta',visc} = 6\pi\eta R_i \delta^{\alpha'\beta'}. \quad (10)$$

The cell-to-cell damping coefficient is,

$$\begin{aligned} \gamma_i^{\alpha'\beta',ad} = & \gamma^{max} \sum_{j \in NN(i)} (A_{ij} \frac{1}{2} (1 + \frac{\vec{F}_i \cdot \vec{n}_{ij}}{|\vec{F}_i|}) \times \\ & \frac{1}{2} (c_i^{rec} c_j^{lig} + c_j^{rec} c_i^{lig})) \delta^{\alpha'\beta'}. \end{aligned} \quad (11)$$

The indices α' and β' represent cartesian co-ordinates. Viscosity of the medium surrounding the cell is denoted by η and γ^{max} is the adhesive friction coefficient.

Cell birth, apoptosis and dormancy : We implement a mechanical feedback on cell growth and division on the basis of the local forces experienced by a cell. Depending on the local forces, a cell can either be in the dormant (D) or in the growth (G) phase. The effect of the local cellular microenvironment on proliferation, a collective cell mechanical effect, is taken into account through the pressure experienced by the cell (p_i). We refer to p_i as pressure because it has the same dimensions, and models the mechanical sensitivity of cell proliferation to the local environment. The total pressure (p_i) on the i^{th} cell is,

$$p_i = \sum_{j \in NN(i)} \frac{|F_{ij}|}{A_{ij}}, \quad (12)$$

The non-zero value of p_c is the source of biomechanical feedback that regulates cell growth.

There are several ways to compute pressure in cell collectives (for a review see Ref.¹²). Here, we define pressure following previous studies^{5,13}. These studies produced quantitative agreement with experiments on the dynamics of multicellular spheroid growth¹².

REFERENCES

- ¹Siefert, J. C., Clowdus, E. A. & Sansam, C. L. Cell cycle control in the early embryonic development of aquatic animal species. *Comparative Biochemistry and Physiology Part C: Toxicology & Pharmacology* **178**, 8–15 (2015).
- ²Puliafito, A. *et al.* Collective and single cell behavior in epithelial contact inhibition. *Proceedings of the National Academy of Sciences* **109**, 739–744 (2012).
- ³Kimmel, C. B., Ballard, W. W., Kimmel, S. R., Ullmann, B. & Schilling, T. F. Stages of embryonic development of the zebrafish. *Developmental dynamics* **203**, 253–310 (1995).
- ⁴Keller, P. J., Schmidt, A. D., Wittbrodt, J. & Stelzer, E. H. Reconstruction of zebrafish early embryonic development by scanned light sheet microscopy. *science* **322**, 1065–1069 (2008).
- ⁵Schaller, G. & Meyer-Hermann, M. Multicellular tumor spheroid in an off-lattice voronoi-delaunay cell model. *Physical Review E* **71**, 051910 (2005).
- ⁶Galle, J., Loeffler, M. & Drasdo, D. Modeling the effect of deregulated proliferation and apoptosis on the growth dynamics of epithelial cell populations in vitro. *Biophysical journal* **88**, 62–75 (2005).
- ⁷Kane, D. A. & Kimmel, C. B. The zebrafish midblastula transition. *Development* **119**, 447–456 (1993).
- ⁸Montel, F. *et al.* Stress clamp experiments on multicellular tumor spheroids. *Physical review letters* **107**, 188102 (2011).
- ⁹Malmi-Kakkada, A. N., Li, X., Samanta, H. S., Sinha, S. & Thirumalai, D. Cell growth rate dictates the onset of glass to fluidlike transition and long time superdiffusion in an evolving cell colony. *Physical Review X* **8**, 021025 (2018).
- ¹⁰Drasdo, D. & Höhme, S. A single-cell-based model of tumor growth in vitro: monolayers and spheroids. *Physical biology* **2**, 133 (2005).
- ¹¹Pathmanathan, P. *et al.* A computational study of discrete mechanical tissue models. *Physical biology* **6**, 036001 (2009).
- ¹²Van Liedekerke, P., Palm, M., Jagiella, N. & Drasdo, D. Simulating tissue mechanics with agent-based models: concepts, perspectives and some novel results. *Computational particle mechanics* **2**, 401–444 (2015).
- ¹³Byrne, H. & Drasdo, D. Individual-based and continuum models of growing cell popula-

tions: a comparison. *Journal of mathematical biology* **58**, 657 (2009).